AGU PUBLICATIONS

Tectonics

RESEARCH ARTICLE
10.1002/2016TC004455

Key Points:
- A metamorphic and structural zonation of a HP/LT metamorphic belt in Central Qiangtang of North Tibet was unraveled
- A two-step exhumation model was formulated after a compilation of radiometric results and reappraisal of phengite ages
- Extensional detachment faulting was substantiated to account for the exhumation mechanism of HP-LT rocks in Central Qiangtang

Supporting Information:
- Supporting Information S1
- Table S1
- Table S2
- Table S3
- Table S4
- Table S5
- Table S6

Correspondence to:
X. Liang,
liangx@cugb.edu.cn

Citation:
Liang, X., G. Wang, B. Yang, H. Ran, Y. Zheng, J. Du, and L. Li (2017), Stepwise exhumation of the Triassic Lanling high-pressure metamorphic belt in Central Qiangtang, Tibet: Insights from a coupled study of metamorphism, deformation, and geochronology, *Tectonics*, *36*, 652–670, doi:10.1002/2016TC004455.

Received 25 DEC 2016
Accepted 6 MAR 2017
Accepted article online 9 MAR 2017
Published online 10 APR 2017

Stepwise exhumation of the Triassic Lanling high-pressure metamorphic belt in Central Qiangtang, Tibet: Insights from a coupled study of metamorphism, deformation, and geochronology

Xiao Liang[1,2], Genhou Wang[1], Bo Yang[1,3], Hao Ran[1], Yilong Zheng[1], Jinxue Du[1], and Lingui Li[1]

[1]School of Earth Sciences and Resources, China University of Geosciences, Beijing, China, [2]Research School of Earth Sciences, Australian National University, Canberra, ACT, Australia, [3]Centre for Tectonics, Resources and Exploration, University of Adelaide, Adelaide, South Australia, Australia

Abstract The E-W trending Central Qiangtang metamorphic belt (CQMB) is correlated to the Triassic orogeny of the Paleo-Tethys Ocean prior to Cenozoic growth of the Tibetan Plateau. The well-exposed Lanling high-pressure, low-temperature (HP-LT) metamorphic complex was chosen to decipher the process by which it was exhumed, which thereby provides insights into the origin of the CQMB and Qiangtang terrane. After a detailed petrological and structural mapping, three distinct N-S-trending metamorphic domains were distinguished. Microscopic observations show that core domain garnet (Grt)-bearing blueschist was exhumed in a heating plus depressurization trajectory after peak eclogitic conditions, which is more evident in syntectonic vein form porphyroblastic garnets with zoning typical of a prograde path. Grt-free blueschist of the mantle domain probably underwent an exhumation path of temperature increasing and dehydration, as evidenced by pervasive epidote veins. The compilation of radiometric results of high-pressure mineral separates in Lanling and Central Qiantang, and reassessments on the published phengite data sets of Lanling using Arrhenius plots allow a two-step exhumation model to be formulated. It is suggested that core domain eclogitic rocks were brought onto mantle domain blueschist facies level starting at 244–230 Ma, with exhumation continuing to 227–223.4 Ma, and subsequently were exhumed together starting at 223–220 Ma, reaching lower greenschist facies conditions generally after 222–217 Ma. These new observations indicate that the CQMB formed as a Triassic autochthonous accretionary complex resulting from the northward subdcution of the Paleo-Tethys Ocean and that HP-LT rocks therein were very probably exhumed in an extensional regime.

1. Introduction

High-pressure, low-temperature (HP-LT) metamorphic rocks usually form in paleo-oceanic subduction zones and can shed lights on the tectonic coupling of oceans and continents in convergent orogens through time [*Tsujimori et al*., 2006; *Agard et al*., 2009; *Lister and Forster*, 2016]. Although the HP-LT metamorphic rocks in Central Qiantang were first reported a century ago by *Hening* [1915], geologists began to unravel their metamorphism, geochronology, and tectonic origin since the late 1990s [*Bao et al*., 1999; *Yin and Harrison*, 2000; *Kapp et al*., 2003; *Li et al*., 2006; *Zhang et al*., 2006a, 2006b; *Zhai et al*., 2011a, 2011b]. Blueschists were discovered as giant structural blocks within the Central Qiangtang metamorphic belt (CQMB) and are distributed from Gangma Co [*Deng et al*., 2000; *Zhai et al*., 2009b] and Hongjishan [*Lu et al*., 2006; *Tang and Zhang*, 2014] in the west to Guoganjianianshan/Pianshishan [*Li et al*., 2006] and Lanling/Qomo Ri in the middle [*Li et al*., 2008; *Zhai et al*., 2009a] and to Naruo, Qiagelela, and Caiduo Caka in Shuanghu in the east [*Li*, 1987; *Bao et al*., 1999; *Zhu et al*., 2010]. Eclogite was also found in the core of the high-pressure metamorphic belt in Gangma Co [*Zhai et al*., 2009b, 2011a], Pianshishan [*Li et al*., 2006], and Guoganjianianshan [*Dong and Li*, 2009]. Despite the above intense studies, the origin, evolution, and tectonic significance of these HP-LT metamorphic rocks and the entire CQMB remain widely debated (cf. *Zhao et al*. [2014] and *Pullen and Kapp* [2014] in more details). Two radically different hypotheses interpret the CQMB as follows: (1) as an autochthonous accretionary complex between South Qiangtang and North Qiangtang terranes as a result of the Triassic northward subduction of Paleo-Tethys Ocean beneath North Qiangtang [*Li*, 1987; *Li et al*., 1995, 2008; *Zhang et al*., 2006b, 2010a; *Zhai et al*., 2011a, 2011b; *Liu et al*., 2011; *Liang et al*., 2012; *Zhao et al*., 2014] and (2) as an allochthonous mélange belt alternatively from the Jinsha suture ~200 km to the north (see the

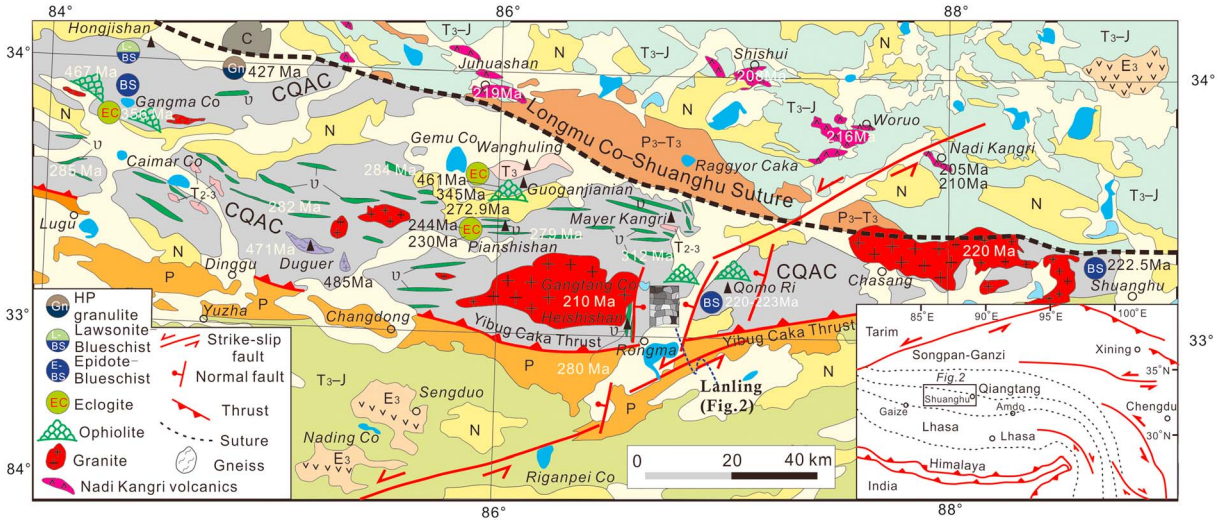

Figure 1. Simplified geological map of the Central Qiangtang and the Longmu Co–Shuanghu suture (with an integration of new discoveries). From north to south, the tectonic framework of Central Qiangtang can be primarily classified into North Qiangtang Late Paleozoic–Jurassic sediments; the Central Qiangtang accretionary complex (CQAC/CQMB) including Ordovician gneiss, Yibug Caka thrust fault, and Permian sediments; and South Qiangtang Late Triassic–Jurassic sediments. The Nadi Kangri volcanic rocks in the south margin of North Qiangtang, Gangtang Co granite batholith, high-pressure metamorphic rocks, ophiolite relics, and rift-related mafic dyke swarm within the CQAC/CQMB are specifically marked.

inset in Figure 1), forming in the process that a shallow dipping Paleo-Tethys oceanic slab subducted southward along the Jinsha suture, then underthrusted far beneath the uniform Qiangtang terrane, and was ultimately exhumed in an intracontinental setting by crustal extensional detachment at Late Triassic [*Yin and Harrison*, 2000; *Kapp et al*., 2003; *Pullen and Kapp*, 2014]. Essentially, this ongoing controversial subject plays a crucial role in uncovering the tectonic history of Tibet and establishing the initial boundary conditions for Cenozoic growth of the Tibetan Plateau [*Zhao et al*., 2014; *Pullen and Kapp*, 2014].

The HP-LT rocks include rather abundant information on the evolution of an oceanic subduction zone in that its exhumation process and mechanism is, a priori, an idea indicator for the genesis of the whole mélange belt or accretionary complex [*Tsujimori et al*., 2006; *Agard et al*., 2009]. The mode of exhumation of the HP-LT metamorphic rocks within the CQMB still remains poorly understood. To summarize, previous researches have predominantly focused on the more highly metamorphosed rocks in the core of the HP-LT metamorphic belt and only revealed their characteristics of petrology, mineralogy, and geochronology [cf. *Bao et al*., 1999; *Kapp et al*., 2003; *Lu et al*., 2006; *Zhang et al*., 2006a, 2006b; *Li et al*., 2006, 2008; *Pullen et al*., 2008; *Zhai et al*., 2009a, 2009b, 2011a, 2011b; *Dong and Li*, 2009; *Dong et al*., 2009; *Zhang et al*., 2010a, 2010b; *Liu et al*., 2011; *Tang and Zhang*, 2014]. The Lanling HP-LT metamorphic belt, which is situated in the middle of the E-W trending Central Qiangtang HP-LT metamorphic belt (Figures 1 and 2), preserves complete types of metamorphic rocks, continuous rock exposures, and clear geological boundaries [*Kapp et al*., 2003; *Li et al*., 2008; *Zhai et al*., 2009a], which largely facilitates a study on unraveling the exhumation processes of those HP-LT metamorphic rocks in Central Qiangtang of North Tibet.

In this paper, the intermediately and slightly metamorphosed rocks in the outer Lanling HP-LT metamorphic belt are also taken into account. More importantly, we present a comprehensive study which correlates the relationship between metamorphism and deformation, provides detailed structural determinations of the contacts between heterogeneous metamorphic domains, and carefully interprets radiometric dating data. The aims are to (1) determine the subduction and exhumation processes of the Lanling HP-LT metamorphic belt and (2) compare it to the adjacent HP-LT metamorphic terranes in Central Qiangtang and try to make an evaluation on the tectonic origin of the CQMB.

2. Geological Background

The Qiangtang basin in northern Tibet is sandwiched between the Jinsha and Bangong-Nujiang suture zones. Both geophysical and topographic data indicate that it is dominated by an E-W trending uplift realm that

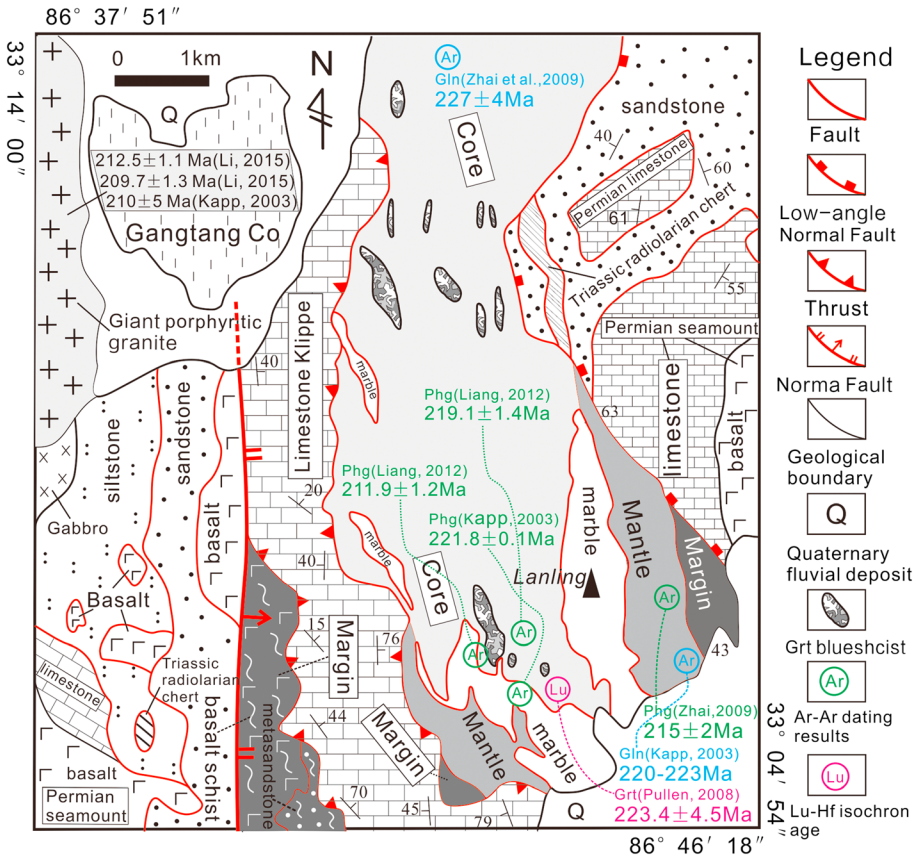

Figure 2. Sketched geological map showing the symmetric structure of Lanling HP-LT metamorphic belt and its surrounding Permian–Triassic mélange which was very shallow metamorphosed. Note that the metamorphic/structural zonation such as core, mantle, and margin domains was deduced from a detailed structural and petrological mapping (see Figure S1). The composition of the surrounding mélange was also derived from a geological mapping where rock ages are indicated by various fossils.

separates the North Qiangtang and South Qiangtang depressions on both sides [*Zhao and Li*, 2000; *Lu et al*., 2001]. The so-called central uplift in the Gangma Co-Gemu-Guoganjianian-Pianshishan-Mayer Kangri-Qomo Ri-Shuanghu areas is rather consistent with the Triassic Central Qiangtang accretionary complex belt [*Liang et al*., 2012] in terms of its morphology and distribution range (Figure 1). The two subordinate basins carry extensive outcrops of Triassic–Jurassic marine sedimentary strata that were unconformably overlain by similar continental sediments after the Cretaceous [*Wang et al*., 2001, 2004]. This complex has been determined to be a Triassic accretionary complex, with the youngest age as Late Triassic and can be attributed to the subduction and closure of the Paleo-Tethys Ocean in Central Qiangtang [*Wang et al*., 2009; *Liang et al*., 2012]. The Late Triassic Longmu Co-Shuanghu suture [*Li et al*., 1995, 2009], which is located on the north of Mayer Kangri Snow Mountain (Figure 1), confines the northernmost margin of the complex [*Liang et al*., 2012, 2015].

The Ladling HP-LT metamorphic belt, which extends in the N-S direction, is embedded in the surrounding nearly unmetamorphosed or subgreenschist facies metamorphosed Triassic accretionary complex (Figure 2). *Yin and Harrison* [2000] and *Kapp et al*. [2003] considered this HP-LT metamorphic belt as the footwall of a Late Triassic–Early Jurassic metamorphic core complex. It was later clarified not to be generated from the southward flat-slab subduction of the Paleo-Tethys Ocean along the Jinsha suture ~200 km to the north [*Zhang et al*., 2006a, 2006b, 2010a; *Zhai et al*., 2011b; *Tang and Zhang*, 2014] but instead indicates a Triassic subduction zone of Paleo-Tethys Ocean in Central Qiangtang because the rock assemblage, which majorly consists of siliciclastic rocks and within-plate oceanic island basalts-type alkalic metabasalt, can be obviously distinguished from those of the Jinsha suture [*Zhang et al*., 2006b]. Furthermore, both the blueschist facies metamorphic rocks at Lanling and the very shallow metamorphosed surrounding rocks on western and

eastern flanks share a common protolith assemblage, which is interpreted as derived from the south Qiangtang terrane [*Liang et al*., 2012]. Such inferences are also supported by the similarity of the detrital zircon age spectra obtained from metasandstones included within both sequences, implying a tectonic affinity with Tethys Himalaya far to the south [*Zhao et al*., 2014].

Generally, the architecture of Lanling HP-LT metamorphic belt and its surrounding is characterized by a symmetric distribution of rock assemblage (Figure 2). On the western flank, block-in-matrix structure is showed by that Late Carboniferous–Early Permian rift-related mafic dykes [*Zhai et al*., 2013], Early Permian seamount remnants comprising fusulinid fossil-bearing limestone and pillow basalt [*Deng et al*., 1996; *Liang et al*., 2012] and Middle to Late Triassic radiolarian cherts [*Deng et al*., 1996; *Li et al*., 1997] all emerge as rigid slices randomly distributed within the Late Carboniferous–Middle Permian submarine fan clastic rocks [*Liang et al*., 2012]. The surrounding mélange on the eastern flank also displays a rather similar rock assemblage consisting of Early Permian seamount consisting of pillow basalt and fusulinid fossil-bearing limestone, Middle to Late Triassic radiolarian cherts, and limestone and thick sandstone layers.

3. Geometry and Metamorphism

The Lanling HP-LT metamorphic belt is characterized by medium- and high-P/T metamorphic facies series and majorly contains a rock combination of siliciclastic rocks, basites, and marbles. Generally, it shows a gradually descending metamorphic grade, ranging from retrograded eclogite facies rocks near the center, epidote (Ep)-blueschist facies near the periphery, and lower greenschist facies around the margin; for simplicity, we refer to these different domains as core, mantle, and margin, respectively (Figures 2 and 3). Although multistage deformations have probably created rather complex structural geometries, these HP rocks generally demonstrate a visible variability and clear zonation in the transverse direction (Figures 2 and 3). Each metamorphic type was structurally mingled with laterally bounded rocks to display a mélange-like morphology (Figure 3e), while the interior lithologies, which were either sedimentary or mafic magmatic, were sheared and then stretched into repetitive bands (e.g., phyllite and amphibolite, marble and blueschist, and phengite (Phg)-schist and retrograde eclogite) (Figure 3).

3.1. Metamorphic Zonation of HP Rocks and Their Relationships

After studying the replacement relationships of rocks and mineral assemblages in detail based on both field observations and microscopic analyses (see the sampling loci in Figure S1 in the supporting information), we identified three major types of metamorphic facies that reflect burial to contrasting depths: garnet (Grt)-bearing blueschist, Ep-blueschist, and low greenschist/amphibolite (Figure 3). These metamorphic types are distributed in approximately N-S trending zones on length scales of kilometers, sharing a similar extension with the entire Lanling belt.

Grt-bearing blueschists occur in the core area of the Lanling HP belt and are unexceptionally embedded within a Grt-bearing leucoschist matrix with lesser white marbles (Figures 3a and 3b). Generally, the dark garnet-bearing masses were all stretched and flattened into N-S trending lathy lenses, which is concordant with the schistosity of the surrounding weak matrix (Figure 3b), and indicate intense structural stretching during exhumation. In the mantle domain, Ep-blueschists or metabasalts are extensively exposed and collage with finely crystalline marble or leucoschist (Figures 3c and 3d). The mantle blueschists differentiate themselves from those in the core according to either the absence of any porphyroblastic garnets and their corresponding pseudomorphs or the common appearance of bulk basalt relicts that are wrapped by blueschist lamina (Figure 3d). On the eastern and western flanks of Lanling, blueschist and marble were strongly sheared into rhythmic parallel layering or isoclinal folds, displaying repetitive dark blue or white colors (Figure 3c). From a large spatial view on the scale of several kilometers, these two high-pressure rock varieties are enclosed in a low greenschist facies metamorphosed sequence (Figures 2 and S1), which mainly includes siltstone, quartz sandstone, and basite lenses consisting of basalt and lesser gabbro/diabase (Figures 3e and 3f). An evident structural boundary exists that separates blueschist and lower greenschist domains, whereas this boundary was discovered to be a transition zone on a smaller outcrop scale in terms of the mingling of blueschist/phengite schist and phyllite/actinolite schist (Figure 3e). This phenomenon probably demonstrates a strong ductile shearing when the blueschists were exhumed at depth.

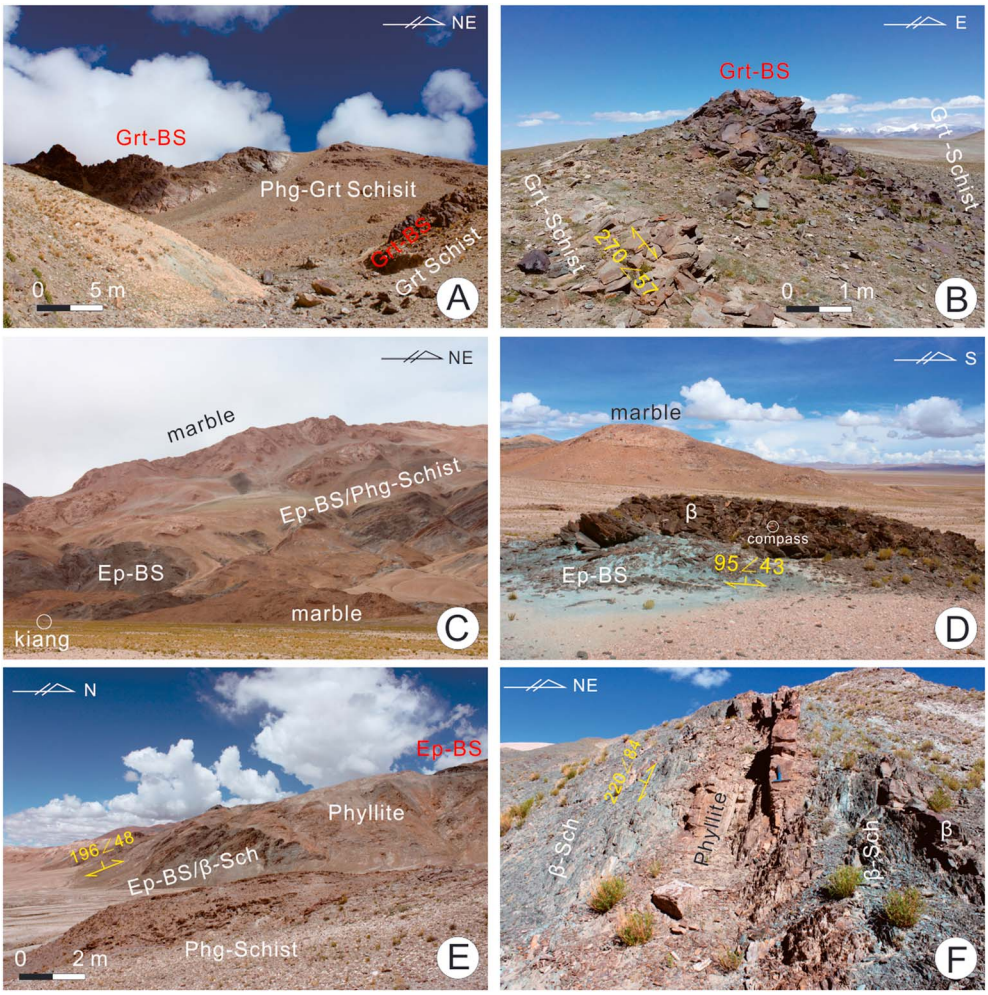

Figure 3. Different rock varieties traversing the N-S trending Lanling high-pressure metamorphic belt. (a and b) Core domain: Grt-bearing blueschist lenses enclosed by the Grt-bearing leucoschists. (c) Mantle domain: Ep-blueshist, marble and lesser Phg-schist collaged with each other to show a repetitive structural layering. (d) Lower left corner of Figure 3C: Ep-blueschist enwrapping lens-like basalt relict to indicate a deformation partitioning. (e) Inner margin domain: Ep-blueschist/Phg-schist mingling with phyllite/basaltic schist. (f) On the north of Figure 3e: outer margin domain: lower greenschist facies metamorphosed phyllite/basalt.

3.2. Metamorphic Characteristics of Each Domain

3.2.1. Core Domain

Grt-bearing blueschists were randomly dispersed in the penetratively foliated siliciclastic rock matrix as giant lenses whose sizes range from ~1 to ~100 m wide (Figures 3a and 3b), displaying a structural mode resembling rigid boudinage in ductile shear zones. Commonly, these individual masses share an analogous mineral combination of Ep + glaucophane (Gln) + Grt + Phg + rutile (Rt), which was likely derived from eclogites after a fluid-infiltrating reaction according to the Ep-enriched bands and garnet polycrystalline veins (Figures 4a and 4b). Epidote and lesser zoisite/clinozoisite usually appear as either swarms or parallel bands (Figures 4c and 8), and a large portion of them are characterized by Gln intergrowths or inclusions.

The occurrence of garnet porphyroblasts is similar to that of epidote, namely, polycrystalline veins or irregular dots within the bulk rock (Figures 4a and 4b). Although rimmed and corroded by chlorite and albite (Figures 4d and 8), euhedral hexagonal Grts had overlapped the matrix mineralogical aggregates, indicating a syntectonic or posttectonic porphyroblast origin compared to the epidote-blueschist facies conditions of Gln/Ep matrix (Figure 4c). This phenomenon is also demonstrated by a truncating contact with linearly oriented matrix minerals, which construct a pervasive foliation in the matrix (Figure 4c). In fact, these minerals more likely evolved from dehydrating metamorphism, which is inferred not only from the macroscopic

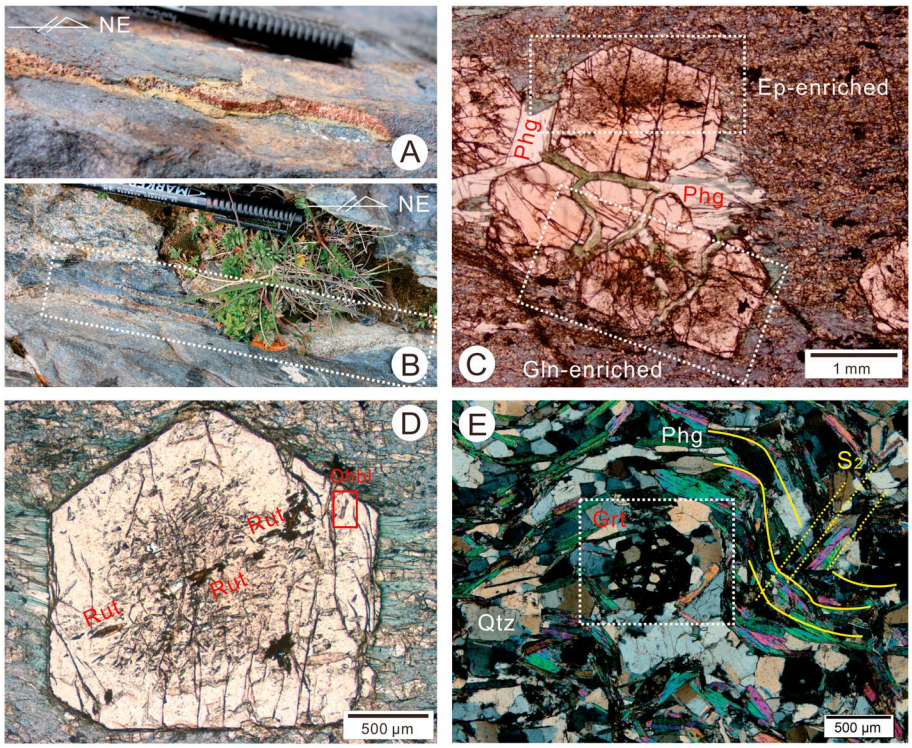

Figure 4. Photographs showing the polycrystalline garnet vein, mineral combination, and syntectonic porphyroblast of the core domain Grt-blueschist (sample L8-13-DB12) and its surrounding leucoschist (sample 14014). (a and b) Phg-Grt veins on the macroscale and the mineralogical zoning (close-up of Figure 3a). (c) Photomicrograph of Figure 4b showing Grt veins and different mineralogical bands (PPL); note the unevenly distributed inclusions within the euhedral Grt. (d) A single garnet dot situated in matrix of tiny Gln and rod-like Ep, displays a clear core, inclusion-enriched mantle and inclusion-scarce margin (PPL). (e) Posttectonic Grt porphyroblast and polycrystalline Qtz bands in the host leucoschist of Grt-blueschist (CPL).

polycrystalline veins but also from the microscopic scenario, in which a sharp quantitative decrease in mineral inclusions occurs when garnet is situated in the middle of the vein space (Figure 4c). Moreover, the vein-residing porphyroblastic Grts are inclined to display a relatively clean interior and contain little inclusions, whereas Grts outside these veins always developed apparent mineralogical contours, which imply episodic growth pulses (Figures 4c and 4d). Three segments could be classified, such as an inclusion-abundant core that occasionally bears a relatively clean center and a clear margin with sparse mineral dots (Figures 4d, 7, and 8). The grain size of the Ep/Gln inclusions progressively increases on the whole from the center to rim (Figures 4d, 7e, and 8), which probably indicates an increasing temperature during growth. This evidence refutes the hypothesis by *Liu et al.* [2011] that the garnets were maintained only as a result of lawsonite (Lws)/Ep eclogitic conditions.

The host leucoschist, which basically includes a mineral combination of Phg + quartz (Qtz) + Grt + calcite (Cal), experienced penetrative ductile deformation. Qtz grains that partially retained pinning structures resulted from grain boundary migration recrystallization (GBM), which were mostly replaced by foam structures because of static recrystallization (Figure 4e), but slightly overprinted by later lower greenschist level deformations, e.g., wavy extinction or bulging minor grains in the rims. Syntectonic Grt porphyroblasts with a maximum diameter of 1 cm are characteristic of asymmetric pressure-shadow structures and coherent S- or Z-shaped fabrics, which consist of quartz bands both inside and outside the Grts and show an evident simple shear rotation. However, posttectonic Grt porphyroblast, which developed extraordinary euhedral polygons with a smaller size of ~0.5 mm, displays little structural disturbance from the matrix fabrics (Figure 4e).

3.2.2. Mantle Domain

Compared to the core domain, the mantle exhibits relatively low temperature metamorphic conditions, which is supported not only by the scarcity of Grt porphyroblasts and their retrograde pseudomorphs but also the common emergence of basaltic relics inside well-foliated epidote-blueschists (Figure 3d). Despite

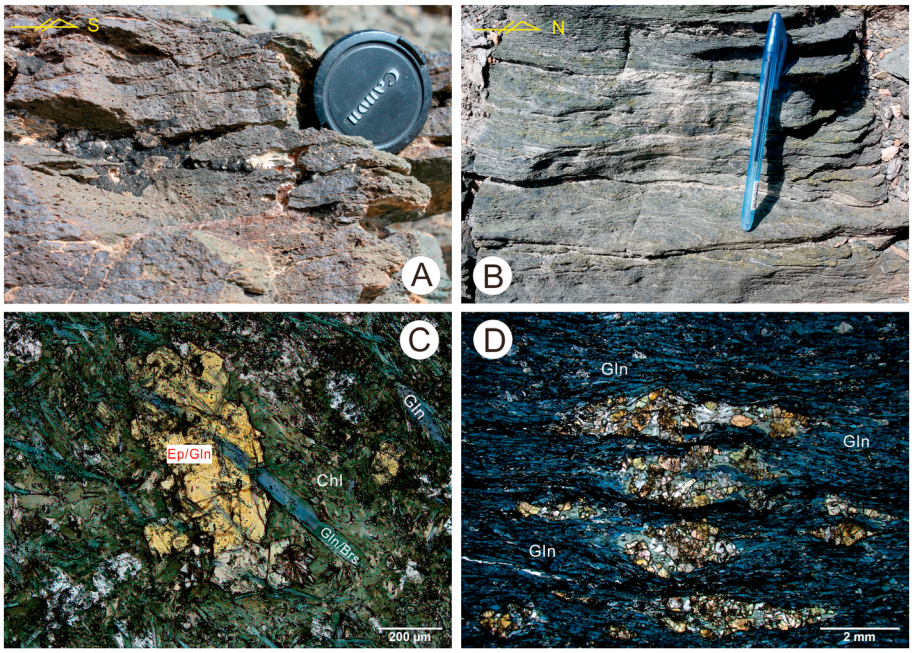

Figure 5. Photographs depicting the metamorphic features of Ep-blueschist in the inner mantle domain. (a) A foliated basalt bulk (samples 14006) with penetrative original vesicular structure (a close-up for Figure 3d). (b) Ep-blueschist with the green Ep clusters either as aggregated masses or folded veins. (c) Intergrowth of nearly euhedral EP and Gln fibers; tiny Ep grains were also founded populating within Gln (samples 14007, PPL) (see Figure S2 and Table S1 for EPMA results of mineral compositions). (d) Porphyroclasts of Ep/Czo aggregates enclosed by oriented Gln rods (PPL).

experiencing a blueschist facies metamorphism at depth according to sparsely distributed Gln grains, the relic basaltic bulks still preserved the original lava textures, such as vesicular/amygdaloidal structures, and display the deformation partitioning together with the surrounding blueschist bands (Figures 3d and 5a). Clinopyroxene or orthopyroxene that had been ruptured into porphyroclasts was preserved in the basaltic remnants, which also discriminates mantle blueschist from core Grt-blueschist with a thorough erasure of magmatic textures.

Generally, epidote-blueschist, leucoschist, and marble collaged with each other in mélange form (Figure 3c), despite that a few Grt-bearing blueschist, were also found incorporated with them in the contact zone as a result of the tremendous ductile shearing. Whether in east or southwest flank of Lanling HP belt, blueschists share a mineral assemblage of Ep + Gln + albite (Ab) + Cal and accessory titanite (Ttn) + Rt (Figures 5c and 5d). The prevalent intergrowths of epidote and glaucophane indicate their metamorphic facies as epidote-blueschist (Figure 3c). Furthermore, the abundant Ep and lesser Zo/clinozoisite (Czo) aggregates that appear in polycrystalline veins or scattered dots within the rock mass probably imply a hydrated metamorphic scenario (Figures 5b and 5d). Additionally, Ab and lesser Cal universally occur as syntectonic porphyroblasts with eye or boudinage structures that contain many Gln/Ep inclusions.

Although Grts could be locally discovered in the leucoschist, they mostly occur as posttectonic euhedral porphyroblasts with a diameter of less than ~3 mm. Individual Phg flakes also have a smaller crystal size than that in the core domain (Figure 6d). Additionally, subgrain rotation and bulging are found as the predominant modes of dynamic recrystallization for quartz grains (Figure 6d). These features of the mantle leucoschist therefore indicate obviously lower temperature conditions for the peak metamorphism, which coincides well with the metamorphism of Ep-blueschist. Indeed, specific Grt growth with a temperature as low as 300°C was documented [*Tsujimori et al*., 2006; *Dragovic et al*., 2015], in particular conditions such as a lower X_{Mg} content at which growth would be promoted.

3.2.3. Margin Domain

This domain basically consists of actinolite (Act)-schist/metabasalt, metasandstone, siltstone phyllite, and lesser limestone and actually constitutes the surrounding matrix for the Lanling HP metamorphic belt (Figure 2). Amphibolite slices over 2 m wide were occasionally found to be embedded within the

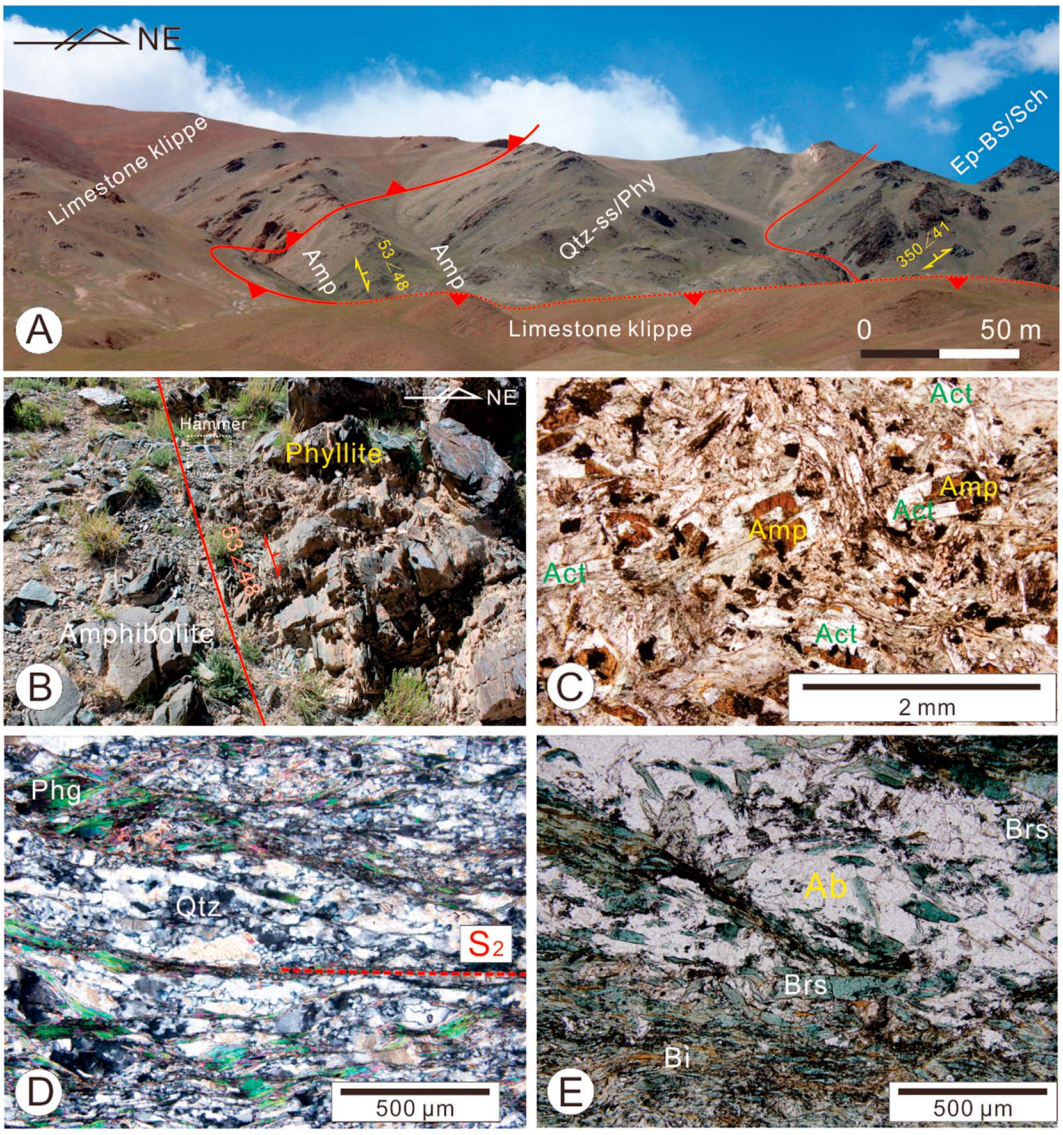

Figure 6. Outcrop-scale contacting relationships between mantle and margin domains and photographs displaying their metamorphic mineral assemblages (see Figure S2 and Table S1 for the EPMA compositional results). (a) A natural transection showing that the mantle domain Ep-blueschist/Phg-schist were surrounded by the margin domain lower greenschist rocks and that both demonstrate a concordant structural trace and were all truncated by a limestone klippe. (b) The amphibolite bulk (sample L-b5 in the lower left of Figure 6a) contacting with siltstone phyllite and sharing a consistent foliation. (c) A photomicrograph of amphibolite showing mineralogical growth zoning comprising Hbl core and Act rim (PPL). (d) A photomicrograph (sample L-b9) showing the foliation replacement demonstrated by Phg fibers and bulging Qtz grains (CPL). (e) Retrograde Ep-blueschist (sample L-b8) with Bi flakes permeating the cleavage domains (PPL).

phyllite/metasandstone (Figures 6a and 6b). The margin domain contacts with the mantle domain through a transitional boundary, in which blueschist/leucoschist and phyllite/limestone intricately collaged with each other in a mélange pattern or parallel interbedding slices (Figure 3e).

Basaltic rocks were strongly foliated but only displayed a greenschist facies metamorphism on both the outcrops and the microscopic view (Figure 3f). Random or semidirected tiny actinolite fibers were prevalently found to wrap euhedral orthopyroxene/clinopyroxene rectangles as long as 0.5–1 mm. Siliciclastic rocks shared an almost invariable mineral aggregate of sericite (Ser) + chlorite (Chl) that enclosed felsic clastics or locally syntectonic pressure-solution Qtz veins. Qtz grains were constantly observed to have experienced a slight bulging recrystallization. Amphibolite (Amp)-schist lenses have been currently recognized at three localities in southwest Lanling, which are structurally coordinated with the foliation of surrounding clastic

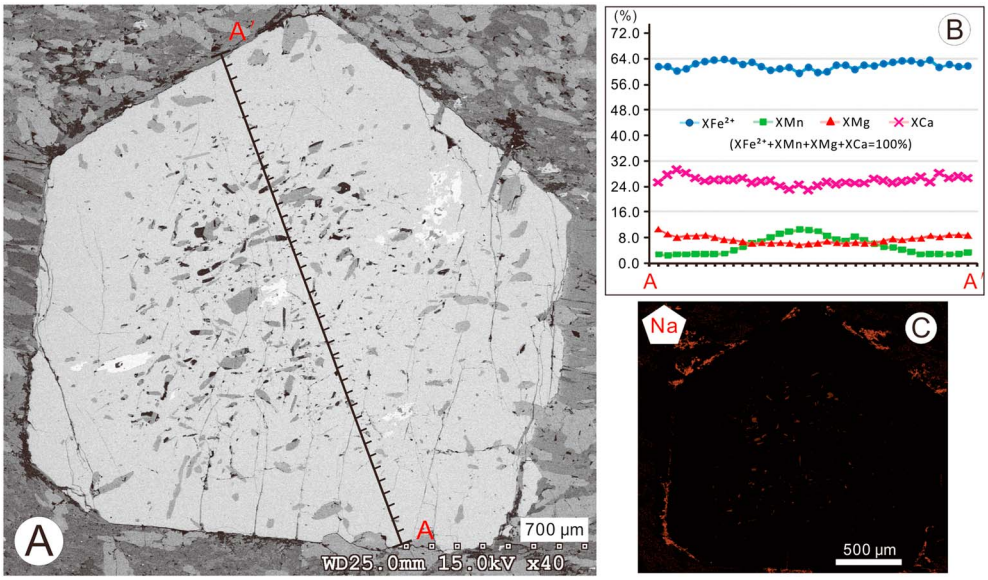

Figure 7. The BSE images and chemical zonings of the Grt porphyroblast corresponding to Figure 4d. (a) A BSE image of the tested Grt with the chemical profile location. (b) The proportion of four Grt end-members (EDXA chemical results are listed in Table S2). (c) A Na-content mapping run by an instrument of QEMSCAN Quanta FESEM.

rocks (Figures 6a and 6b). It shows a mineral assemblage mainly of Ab + Amp + Act (Figure 6c), which indicates epidote-amphibolite facies. Photomicrographs (plane-polarized light) and back-scattered electron (BSE) images all showed clear growth zoning for amphiboles, whose protuberant Mg-Hs/Prg/Krs cores were unexceptionally bordered by the Act strips (Figures 6c and S2).

4. Mineral Compositional Analyses and Pressure-Temperature Estimates

4.1. Garnet Compositional Zoning

Metamorphic porphyroblasts, particularly Grt within HP/ultrahigh pressure (UHP) rocks, preferentially retain their mineralogical morphology and preserve peak metamorphic minerals inside after hydrous corrosion during retrogression [*Tsujimori et al*., 2006, *Dragovic et al*., 2015]. As indicated by the aforementioned microscopic observations, the porphyroblastic Grts in blueschists from the Lanling core domain displayed clear textural zoning. Therefore, we chose a hexagon garnet with abundant mineralogical inclusions (Figure 4d) from sample L8-13-DB12 (Figures 4a and 4b) to implement compositional analyses including both the linear chemical profile and mineralogical mapping in order to uncover its earlier metamorphic growth path (the experimental procedures and working conditions of instruments are detailedly depicted in the supporting information).

4.1.1. X-Ray Linear Chemical Profile

The tested Grt porphyroblast was almandine rich and grossular rich and showed pronounced chemical zoning, which was characterized by the following: (1) Mn components were enriched in the core (e.g., X_{Mn} = ~11%), dramatically decreased toward the rim and leveled off at the margin (e.g., X_{Mn} = ~2%); (2) Mg components were poor in the core (e.g., X_{Mg} = ~6%) and quickly increased outward with a relatively stable gradient except the slight leveling off in the upper end (e.g., X_{Mg} = ~11% in the lower end); (3) Fe components were also poor in the core but fluctuated (X_{Fe} = ~59–62%), rose to a peak in the outer mantle (e.g., X_{Fe} = ~64%) and then dropped intensely despite a moderate climb in the outermost margin (e.g., X_{Fe} = ~61%); and (4) Ca components displayed relatively small variations in general (e.g., X_{Ca} = ~23%) but approached a peak at the margin (e.g., X_{Ca} = ~29%) and then dropped at the rim (e.g., X_{Ca} = ~25%) (Figure 7b). *Liu et al*. [2011] also recognized similar garnet growth zoning to the north of the location of L8-13-DB12 at Lanling, in which the Fe and Mg contents correspondingly rose rimward, while the Mn contents monotonously decreased and Ca components occurred with small changes. However, our Grt porphyroblast specimen demonstrated more detailed and distinctive characteristics with respect to the Fe and Ca contents (Figure 7b).

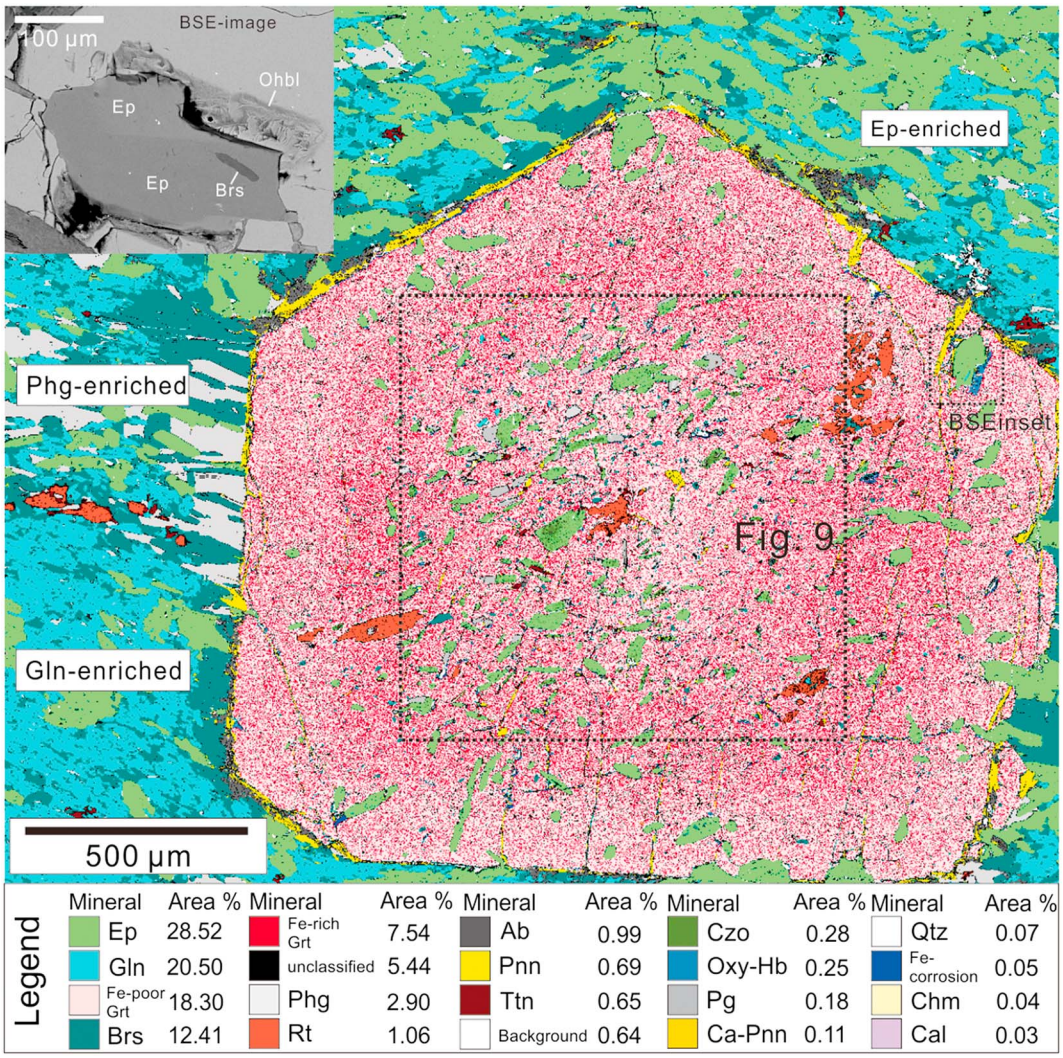

Figure 8. A mineralogical mapping of the same Grt specimen as Figures 4d and 7 showing inclusion varieties and their distribution, which was deduced by a QEMSCAN Quanta FESEM (see Figure S3 for energy spectra of each mineral inclusions). Note that the outside mineral types and their zoning were also presented. The BSE inset in upper left displays the intergrowth of Ep, Brs, and Ohbl.

4.1.2. X-Ray Mineralogical Mapping

A detailed mineralogical map that showed both the interior and external mineralogical distribution coupled with the chemical zoning for the porphyroblastic Grt was obtained (Figure 8). The Grt was located within a phengite abundant zone, which separated Ep-enriched and Gln-enriched bands. Fibriform phengite, glaucophane/barroisite, and epidote grew perpendicularly against the hexagonal boundaries of the crystal to create a pressure-shadow structure. An obvious inclusion-clean outer half provided another support for the genesis of syntectonic porphyroblasts which progressively dilated as the hydrous fluid infiltrated and opened the boundary between the two metamorphic bands. This phenomenon is consistent with that the polycrystalline garnet vein was surrounded by Phg swarms according to both outcrop- and microscopic-scale observations (Figures 4a–4c). Distinct mineral aggregates were detected between the Grt's interior and surrounding matrix (Figure 8), and the distribution of Na contents exhibited a cluster of Na-rich mineralogical inclusions within the Grt's core (Figure 7c). Matrix Gln, Ep, and accessory Rt and Ttn, wherever they occurred, were stretched and rotated to arrange coordinately with nearly identical long axes, which indicates a function of ductile simple shear deformation (Figure 8). This observation is also reflected by the fact that Rt and other inclusions within the Grt were distributed linearly to display a diagonal extension relative to the matrix banding (Figure 8).

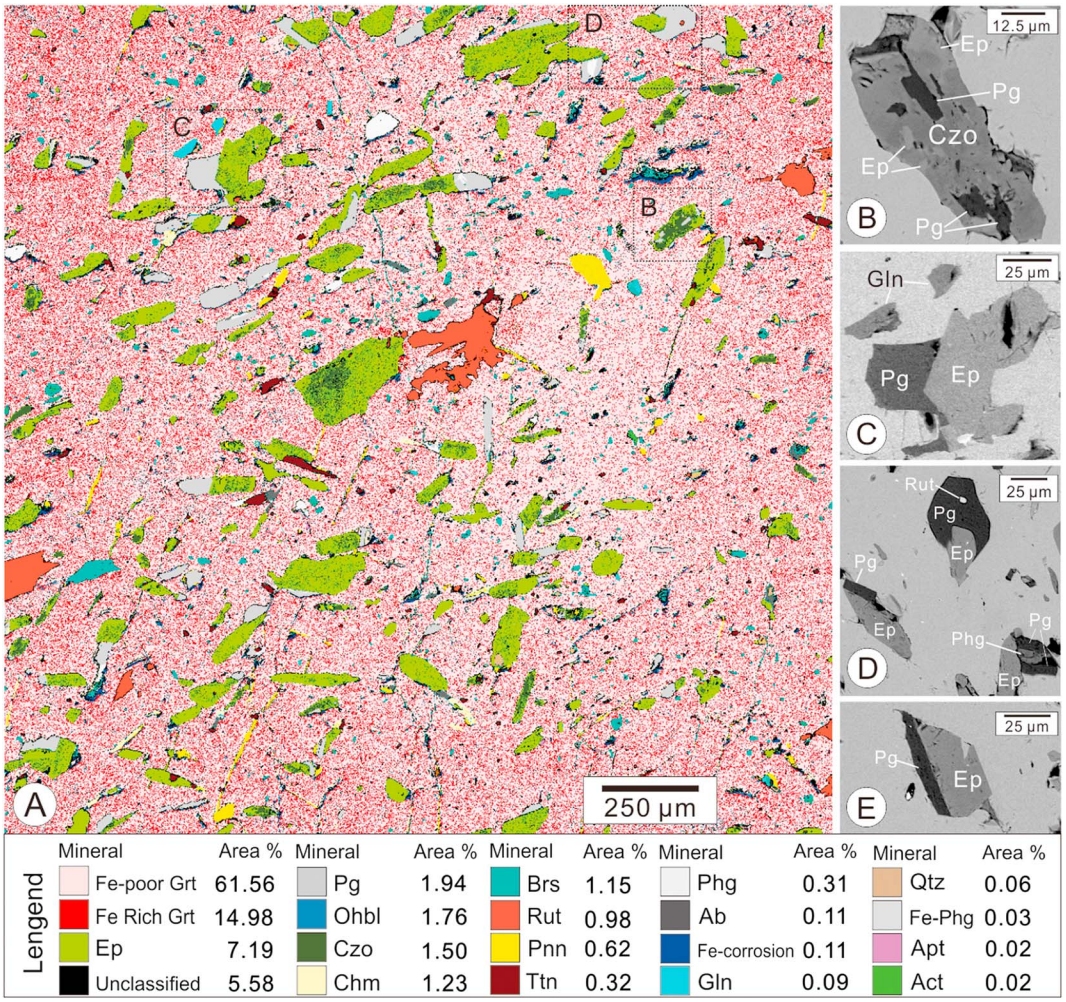

Figure 9. A mineralogical mapping of the Grt core showed in Figure 8, which was deduced by the same instrument of QEMSCAN Quanta FESEM (see Figure S4 for energy spectra of each mineral inclusions). (b–e) The intergrowth of Ep/Czo and Pg and some retrograde rhombic pseudomorphs speculated for Lws (see Table S3 for their EDXA compositions).

Although experienced later corrosion by low-temperature hydrous fluids according to its alteration ring and sparse internal cracks that are dominantly filled with Pnn aggregates, the hexagonal Grt porphyroblast exhibited episodic growth zoning not only in terms of its chemical composition but also in terms of its mineralogical paragenesis (Figures 7b and 8). The iron content is highlighted here (Figure 8), and coincidentally, varying contours were acquired compared to the linear chemical section, which indicated a Fe-rich ring in the mantle area that separated the Fe-poor inner core and outer margin (Figure 7b). The included minerals also generally increased in grain size and could be divided into three growth episodes in terms of their assemblages. The Fe-poor core area was swarming with a variety of minerals, including Ep/Czo, Pg/Phg, Gln/Bar, Rt, Ttn, and Ap, and was bordered by a Fe-rich mantle and Fe-poor margin, both of which showed rapid declines in the inclusion quantities. A specific mapping of the core with higher resolution was performed to precisely constrain the mineralogical relationship (Figure 9). Two distinctive mineralogical intergrowths, such as Ep/Czo and Pg/Phg, differentiated the mineral paragenesis of the core from the external matrix (Figures 9b–9e). Czo was commonly dotted within epidote grains, comprising as much as 60–70 vol % (Figure 9b), while Phg only occupied a rather limited area in Pg flakes (Figure 9d). Furthermore, these two mineral species were found to have been incorporated into each other, showing synchronous growth. A noteworthy discovery was that a few Phg and Ep/Czo inclusions showed rhombic or rectangular shapes, different from other conventional stripes (Figures 9c–9e). Gln occurred as subhedral or xenomorphic grains and was largely replaced by barroisite (Brs) during later retrogression.

Additionally, two later retrograde hydrous corrosion events occurred according to the high-Fe corroded rims that bordered the Gln/Bar, sparse Chm inclusions, and Pnn aggregates filled in the cracks (Figure 9a). The former probably corresponds to the Fe-rich mantle ring, whereas the latter may have occurred afterward when the Pnn aureoles surrounded the porphyroblast (Figure 8). These evidences suggest the episodic decompression growth of the porphyroblastic Grt within sample L8-13-DB12, which could also be verified by the oxyhornblende (Ohbl) that populated the outermost margin (Figure 8 inset).

4.2. Pressure-Temperature Estimate of the Garnet-Bearing Blueschist

Based on the aforementioned Qtz dynamic recrystallization behavior in terms of the pinning and foam structures (Figure 4d), a temperature estimate of ≥500°C could be reckoned for the peak or postpeak metamorphism of the leucoschist surrounding Grt-bearing blueschist (L8-13-DB12). For the pressure-temperature (P-T) calculation of the latter, we applied the Phg geobarometer [*Massonne and Schreyer*, 1987] and Zr-in-rutile geothermometer [*Tomkins et al*., 2007], respectively. Approximately, same temperature results were acquired such as ~497°C for the Rt grains residing either within or outside the Grt porphyroblast (Figures S5–S6 and Table S4). The Si contents in terms of atom per formula unit (a.p.f.u.) of the phengite fibers whether or not distributed within the Grt vein display values of ~3.5 (Table S5 and Figure S7), which indicates a pressure estimate of ~1.3 GPa (Figure S7) for the phase equilibrium of Grt + Gln + Ep + Phg + Rut after plotting on the P-T-Si diagram by *Massonne and Schreyer* [1987].

As depicted above, the tested Grt hexagon coincidentally includes a diagonal distribution of Rt stripes (Figures 4d, 7, and 8) and is hence suitable for the application of Zr-in-rutile geothermometer. Thirteen grains (the localities of laser ablation are shown in Figure S5) were chosen for the acquisition of trace elements using the multiple collector inductively coupled plasma mass spectrometry instrument integrated with a laser device (see the supporting information for the whole experimental process). Due to the irregular grain boundary and limited sizes of Rt inclusions, the laser beam with a diameter of 36 μm would inevitably ablate other inclusions or matrix minerals such as Grt, Brs, and ilmenite (Ilm) (Figure S6). Among them only six got reasonable Zr contents and the other seven abandoned indicate an evident excess of Zr contents because of their aberrant Si and Al rises (Table S4). It is noteworthy that only the laser spot No. 11 almost demonstrates no contamination with a Zr content of 23.82 ppm, while the other five were very slightly mingled with Grt or Ilm or Brs (see both the BSE and reflection light images in Figures S5–S6) and showed exaggerated Zr contents rising by ~10 ppm (Table S4). Given the pressure estimate of ~1.3 GPa, an estimation of ~497°C was derived for the metamorphic temperature of spot No. 11 and a range of ~511 to ~515°C could hence be deemed as the upper limits of the other five ones (Table S4). Taking the Mg-content profile of the Grt (Figure 7b) into account, ~497°C could thereby be interpreted as the median growing temperature between the Grt core and mantle.

4.3. P-T Estimate of Mantle Phengite Schist

The temperature-dependant Qtz dynamic recrystallization behavior and Phg geobarometer [*Massonne and Schreyer*, 1987] were also utilized to indicate the P-T metamorphic condition for the phengite schist (L-b9) from the mantle domain of Lanling (Figures 6d and S2). The widespread subgrain rotation recrystallization behavior of Qtz (Figure 6d) pointed out an obviously lower temperature condition of ≥400°C than the counterpart of the core domain. The Si contents in terms of atom per formula unit (a.p.f.u.) of Phg flakes displayed values of ~3.45 (Table S1), which indicate a pressure of ~1.1 GPa (Figure S7) for the phase equilibrium of Qtz + Phg ± Grt after plotting on the P-T-Si diagram by *Massonne and Schreyer* [1987].

Generally, the inferred metamorphic conditions of Ep-BS facies for the Phg-schist are in accordance with that of the mantle blueschist characterized by a major mineral combination of Gln + Ep + Ab (Figures 5b–5d and 6e).

5. Metamorphic History

A detailed metamorphic and structural trajectory was established for each HP-rock type across Lanling based on the above petrological/mineralogical evolution and their P-T estimates (Figure 10). One particular method, namely, Tectonic Sequence Diagrams [*Foster and Lister*, 2008; *Lister and Forster*, 2016], was adopted to specify the episodic exhumation history of HP rocks in order to delineate the complex mineralogical overprinting (Figure 11).

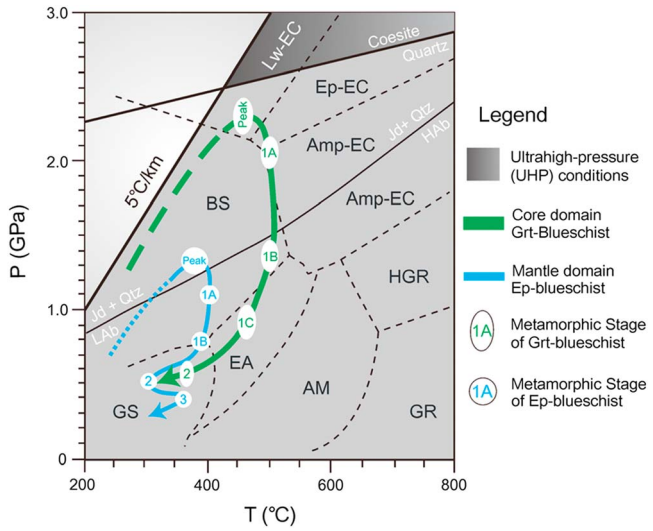

Figure 10. The metamorphic P-T-t paths for the core and mantle blueschists, which were deduced from both the mineralogical evolution and quantitative P-T estimates using the geothermobarometry (the base phase diagram was modified from *Tsujimori et al.* [2006]).

Core domain blueschists showed a more complicated metamorphic process than that of mantle but presented similar retrogression paths when exhumed, i.e., a heating transition into the Ep field followed by pervasive Barrovian-type overprints (Figure 10). Grt-bearing blueschists experienced a heating transition from the Lws field into the Ep field and then quickly depressurized, entering the low greenschist field via the epidote-amphibolite field. The Δ_{1A} phase was retained within the core of the Grt porphyroblast showing a mineral assemblage of Grt + Gln + Pg/Phg + Czo/Ep (Figure 9), and the absence of Lws could be attributed to temperature-sensitive transformation into clinozoisite/zoisite [*Tsujimori et al.*, 2006]. The alternative case of the fluid-unsaturated conditions [*Clarke et al.*, 2006] could hence be precluded. Lws was rarely found in oceanic subduction zones worldwide, so aggregates of Pg + Czo with relict rhombic pseudomorphs would be a good candidate [*Tsujimori et al.*, 2006; *St-Onge et al.*, 2013]. The rising Ca content of the Grt porphyroblast away from the core (Figure 7b) also supports a Lws-consuming process versus conventional Chl-consuming reactions, which usually yield a constant Ca-content trend [*Tsujimori et al.*, 2006 and references therein]. Moreover, the evident hydrous scenario as indicated by the occurrence of garnet swarms within Phg-abundant veins probably points out the breakdown of lawsonite (Figures 4a–4c).

The combination of Grt + Gln + Lws is advocated to have reached the Lws-eclogite facies because omphacite is usually erased by subsequent blueschist retrogression or chemically dependent phase transition of blueschist/eclogite [*Tsujimori et al.*, 2006]. Therefore, we ascribe Δ_{1A} to an Ep-eclogite stage following peak Lws-eclogite facies metamorphism or more likely the transition to the Ep-blueschist facies. The stage of

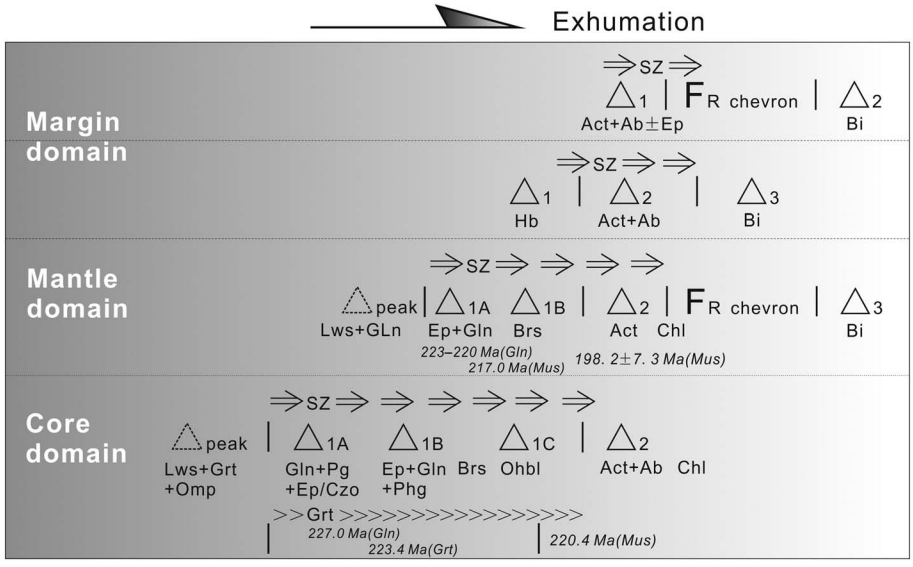

Figure 11. A tectonic sequence diagram displaying the detailed structural and metamorphic evolving history for three metamorphic domains of Lanling HP belt (Note that the episodic mineral generations are underlined).

Δ_{1B}, corresponding to the Fe-enriched ring in the Grt mantle, obviously represents the Ep-blueschist facies stage, which was also reflected by the matrix's Ep/Gln aggregates. The nearly identical P-T estimates of ≥ ~497°C and ~1.3 GPa either for the Grt-Phg vein or its matrix (Figures S5–S7 and Table S4) obviously corroborate this speculation. Additionally, the metamorphic P-T conditions of Δ_{1A} could therefore be constrained as < ~497°C and > ~1.3 GPa. The Grt margin growth Δ_{1c} with Ohbl inclusions (Figures 4d and 8) could be related to the transition from the last HP metamorphism of Δ_{1B} to Barrovian-type greenschist stage of Δ_2. This critical conversion from the former prograde heating phase to an approximately equal decline of pressure and temperature was confirmed by the leveling off or slight rise in Mn-content profile and the inverse Mg content one when approaching the rim (Figure 7b). The pennine (Pnn) and Ab aureole of Δ_2, which bordered the Grt marks fierce hydrous corrosion when the rock was exhumed onto low greenschist or even shallower levels (Figure 8).

The Grt-scarce Ep-blueschists in the mantle domain were probably derived from Lws-blueschist, which prefers very low temperature conditions. The pervasive Ep-group mineral veins that were stretched into stripe- or eye-shaped porphyroclasts support an episodic hydrous reaction, which probably happened as a result of the dehydration of Lws (Figures 5b–5d). This transformation implies a heating path during early exhumation after reaching peak pressure at depth. Δ_{1A}'s Ep-blueschist facies mineral assemblage of Ep/Czo + Gln well corresponds to its counterpart, i.e., the assemblage of Qtz + Phg ± Grt within the Phg-schist and hence share the P-T estimate of ~400°C and ~1.1 GPa (Figure S7). It is noteworthy that Ep-blueschist was significantly corroded by later multiple-staged retrogression. Δ_{1c}'s lower greenschist facies largely overprinted the HP metamorphism and is particularly evident in outcrops, where Ep-blueschists were partially retained as irregular dark blue blocks that were surrounded by green Act schists. Unlike the linearly orientated Ep + Gln fabrics of Δ_{1A}, needle-like actinolites displayed static crystallization because of their random distribution, especially the radial aggregates. Δ_{1B}'s Brs aggregates (Figures 5c and 6e) are similar to Δ_{1C} stage of Grt-bearing blueschist. Δ_{1D}'s Bi growth, which partially corroded the Brs/Act fibers (Figures 6e and S2 and Table S1), may represent a mild heating pulse at shallow depth.

In the margin of Lanling, Δ_{1A}'s low greenschist metamorphism of basites and fine-grained siliciclastic rocks was characterized by invariable mineral combinations of Act + Ab ± Ep and Ser + Qtz ± Chl, respectively. Small amphibolite blocks (Figures 6a–6c), however, demonstrated an Ep-amphibolite facies prior to Δ_{1A}, which probably suggests a heterogeneous isotherm across the accretionary complex. An obvious heating pulse is also evident as shown by the discontinuous Bi flakes that were dispersed in the margin domain rocks.

6. Discussion

6.1. Reinterpretation of Phg Ar-Ar Results by Multidiffusion Domain Modeling

Phg/muscovite (Mus) have proved to be retentive argon reservoirs and are widely used to extract thermal histories when HP metamorphic terranes were exhumed [*Harrison et al*., 2009; *Harrison and Lovera*, 2014; *Foster and Lister*, 2014; *Lister and Forster*, 2016]. Phg and Mus exhibit different closing temperatures (Tc) for Ar diffusion [*Foster and Lister*, 2014], namely, ~550°C [*Lister and Forster*, 2016] and ~350°C [*McDougal and Harrison*, 1999], respectively. Given that several Phg argon radiometric data have been acquired at Lanling [*Kapp et al*., 2003; *Zhai et al*., 2009a; *Liang et al*., 2012], it is surprising to find the lack of attempts to precisely correlate the ^{40}*Ar/^{39}Ar age spectra with the cooling processes of exhumed rocks rather than the apparent "plateau ages." Therefore, we reinterpreted the five published Phg ^{40}Ar-^{39}Ar dating data sets (Table S6) to reassess their implications on the exhumation process by using eArgon program by *Lister and Forster*, 2016. It is noted that no preference is given to the Ar-Ar dating results, and all the hitherto reported Phg age data of Lanling were taken into our account.

Arrhenius plots show evident episodic Phg/Mus growth pulses in a wide stepwise heating ^{40}Ar*/^{39}Ar age span of 222.0–211.9 Ma, and a short interval of 222.0–217.0 Ma generally marks the metamorphic transition from Phg growth to Mus growth (Figures S5 and S6). Two age spectra of Phg separates from Lanling and its surrounding acquired by *Kapp et al*. [2003] both display staircase shapes, which are typical of the mixed degassing mode of multiple Ar-diffusion domains [*Foster and Lister*, 2004, 2014]. Specimen 5-31-99-1c collected on the northeast of Lanling retained a final Phg-growing scenario at 221.3 ± 0.1 Ma according to the age of step 8, which could be regarded as the upper limit of Δ_{1B}, whereas another older, anomalous

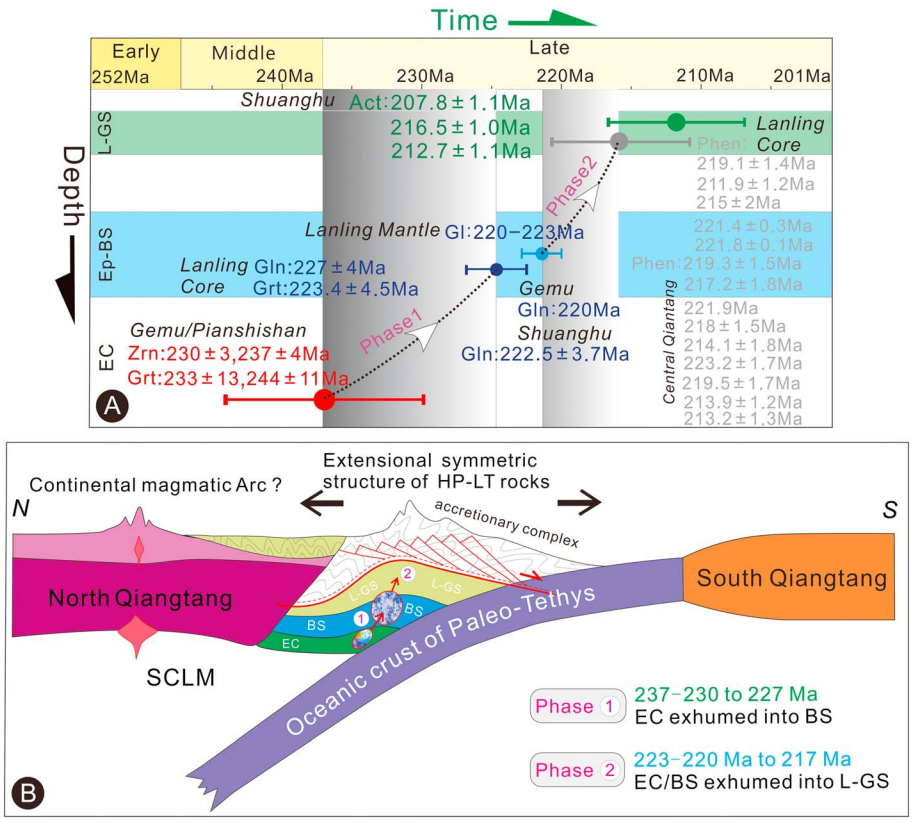

Figure 12. A two-phase exhumation process derived from both the structural/metamorphic evolution of Lanling HP-LT belt and a complete compilation of reported radiometric results of high-pressure minerals from Lanling and Central Qiangtang. (a) The categorization of dating results according to the metamorphic characteristics of each rock varieties; the time span of two exhumation phases was hence indicated. (b) A schematic cartoon demonstrating the exhumation process of HP-LT rocks in Lanling and Central Qiangtang.

age of 227.4 ± 0.5 Ma from step 5 with a low *E* (activation energy) of 40.31 kcal/mol may have recorded an earlier prograde Mus growth (Figure S8). The other specimen (6–30 to 99–2 m) from the Lanling core domain showed a splendid mineralogical transition from an earlier Phg Δ_{1B} age of 222.0 ± 0.1 Ma (step 6) to a subsequent Mus post-Δ_{1B} age of 220.4 ± 0.4 Ma (step 4; Figure S8). The P8 specimen in the Lanling mantle domain from *Zhai et al.* [2009a] demonstrated both an earlier Phg Δ_{1A} age of 217.0 ± 2.5 Ma (step 6) and a later Mus Δ_2 age of 198.2 ± 7.3 Ma (Figure S8). Distinctly, two other specimens in the Lanling core domain from *Liang et al.* [2012] both displayed suitable plateau ages of 219.37 ± 0.26 Ma (P22-16-TW1) and 211.95 ± 0.12 Ma (P22-16-TW3). The Arrhenius plots indicate that the former age constrains the Mus post-Δ_{1B} or Δ_{1c} stage after high-pressure metamorphism, whereas the latter reveals a classic Phg-growing age of Δ_{1B} (Figure S9). The seemingly incompatible late Phg growth until 211.95 ± 0.12 Ma for sample P22-16-TW3 may have been a function of the heterogeneous cooling of thermal conditions within the high-pressure belt.

6.2. Compilation of the Timing of the HP Metamorphic Rocks

Abundant radiometric dating results have been obtained for the HP-LT rocks from Lanling and adjacent regions since ~2000. Here we compile these data to deduce specific geochronological constraints for the exhumation stages of these rocks (Figure 12a). The entire Central Qiantang high-pressure metamorphic belt typifies a Middle to Late Triassic oceanic crust subduction zone [*Kapp et al.*, 2003; *Li et al.*, 2006; *Pullen et al.*, 2008; *Zhang et al.*, 2010b; *Zhai et al.*, 2011a; *Liang et al.*, 2012; *Tang and Zhang*, 2014] as supported by a series of Gln and Phg Ar-Ar, zircon U-Pb, and garnet Lu-Hf isotopic dating data that were acquired in Central Qiangtang's high-pressure metamorphic belt, including Lanling [e.g., *Li et al.*, 1995; *Kapp et al.*, 2003; *Li et al.*, 2006; *Pullen et al.*, 2008; *Zhai et al.*, 2009a, 2011a; *Liang et al.*, 2012]. The eclogites formed under an

estimated pressure of 2.0–2.5 GPa and a wide temperature range of 410–625°C [*Zhang et al*., 2006a; *Dong and Li*, 2009; *Zhai et al*., 2011a], implying a maximum depth of ~80 km for subducted slab-derived oceanic crust [*Agard et al*., 2009]. The Grt Lu-Hf isochron ages (i.e., 244 ± 11 Ma and 233 ± 13 Ma) [*Pullen et al*., 2008] and zircon U-Pb concordant ages (i.e., 237 ± 4 Ma and 230 ± 3 Ma) [*Zhai et al*., 2011a] were obtained for Pianshishan eclogites in Gemu area. Given the closure temperature (T_c) of the U-Pb diffusion system in zircon that could approach as high as ≥850°C [*Cherniak and Watson*, 2001], the above zircon U-Pb ages define a robust timing on the peak metamorphism for eclogite. For the Lu-Hf isotopic system in Grt, the closure temperature (T_c), hitherto, was demonstrated as a significantly varying value due to its dependence on a series of factors such as peak temperature, cooling rate, mineral composition, and grain size and shape [*Scherer et al*., 2000; *Herwartz et al*., 2008]. Despite this complexity, an empirical calculation of ~600°C was deduced after referring the illustration by *Bloch et al*. [2015], according to the speculated relatively rapid cooling history and Grt crystal size of ~1–3 mm for Pianshishan eclogites of Gemu [cf. *Pullen et al*., 2008; *Zhai et al*., 2011a]. It therefore suggests that the above Lu-Hf results reflect Grt growth rather than later cooling ages and that the peak eclogitic metamorphism could be confined to 230–244 Ma.

Although no eclogite has been discovered in Lanling until now, plentiful radiogenic ages were obtained for Grt, Gln, and Phg. *Pullen et al*. [2008] acquired an isochron age of 223.4 ± 4.5 Ma for a garnet separate from Lanling blueschist, which is ~10 Ma younger than zircon SHRIMP U-Pb ages of 230 ± 3 Ma and 237 ± 4 Ma of Gemu eclogite [*Zhai et al*., 2011a]. This distinction corresponds to what we inferred, in which garnets appeared as syntectonic porphyroblasts of the core domain blueschist (Figures 4a–4d), which indicate multiple growing pulses after the peak eclogitic metamorphism (Figures 8 and 10). Moreover, a closer Ar-Ar isotopic age of 227 ± 4 Ma for Gln separates from the core domain was obtained by *Zhai et al*. [2009a]. In light of the metamorphic stages that we established above, the radiometric ages of 223.4 ± 4.5 Ma for Grt and 227 ± 4 Ma for Gln very probably represent the metamorphic stages of Δ_{1A}–Δ_{1C} and Δ_{1B}, respectively. *Kapp et al*. [2003] acquired an Ar-Ar dating age of 220–223 Ma for the Gln separates from the mantle domain at Qomo Ri, which should bound the Δ_{1A} stage after the Lws-blueschist condition.

Generally, time gaps of ~10 Ma could be deduced among three rock species of the HP-LT rocks within the CQMB that were exhumed at varied depths within the subduction channel after carefully comparing the isotopic ages of each individual (Figure 12a).

6.3. Exhumation Process for the Lanling HP Rocks

Oceanic blueschists and eclogites worldwide crop out in short-lived discontinuous exhumation episodes that take place early, late, or incidentally during the oceanic subduction [*Agard et al*., 2009]. Considering the slightly younger Gangtang Co granitic batholith of ~210–212.5 Ma on the west of Lanling (Figure 2) [*Kapp et al*., 2003; *Li et al*., 2015], which is characterized by syncollisional geochemical properties and intruded into the surrounding accretionary complex [*Li et al*., 2015], the HP metamorphic rocks of Lanling and Central Qiangtang typify a late exhumation fashion, similar to New Caledonia, W. Alps [*Agard et al*., 2009]. Based on the detailed P-T-t paths and the compilation of the radiometric dating results (Figures 10 and 11), the exhumation duration for the core domain Grt-bearing blueschist of Lanling from mantle depth in the subduction channel onto the greenschist level is inferred to be ~7 Ma or even a couple of Ma longer (taking the 220.4 Ma as the time mark into greenschist condition), which matches the criteria of < ~15 Ma proposed by *Agard et al*. [2009]. The total time consumption for the exhumation of eclogites from three locations to the west of Lanling, i.e., Gemu [*Li et al*., 2006; *Zhang et al*., 2006a; *Pullen et al*., 2008; *Zhai et al*., 2011a, 2011b], Guoganjianianshan [*Dong and Li*, 2009; *Zhang et al*., 2010b], and Gangma Co [*Zhai et al*., 2009b, 2011a, 2011b], however, may have lasted longer as much as ~13.5 Ma (Figure 12a), if excluding the seemingly deviant Grt age of 244 ± 11 Ma of Gemu eclogite as an outlier, given the probability that Grt could grow either before or after the peak metamorphism [*Dragovic et al*., 2015].

Accordingly, we present a particular stepwise mode that considers the exhumation of the HP rocks in Lanling and contiguous areas of Central Qiangtang based on our comprehensive work and reappraising preexisting data sets (Figure 12b). During the first step (~234–220 Ma), a portion of Lws-eclogites with basaltic protolith were extruded upward and incorporated into the upper Ep-blueschist field at depth of ~40 km, experiencing phase transition from Lws to Czo/Ep. According to the geometries and contact relationships of these three metamorphic domains, the range of ~ 223–227 Ma probably represents the time when the eclogitic rocks

from the core domain exhumed from deep onto the shallower Ep-blueschist level, while 220–223 Ma could be interpreted as their finalizing time into Ep-blueschist conditions.

Continuous exhumation then transited both the eclogites and blueschists from the top of the subduction channel at ~40 km into the accretionary complex. The second step (~220 Ma to ~211 Ma) is reflected by the extensive Barrovian-type retrograde path for all the HP rocks in Lanling, which is in accord with the fact that HP rocks of the core and mantle domains are surrounded by low greenschist/Ep-amphibolite facies metamorphosed rocks of the margin domain. Arrhenius evaluations on the diffusion parameters of muscovite, in particular determining the activation energy (*E*), reveal that the core domain rocks cooled into the greenschist condition generally after 222.0–219.37 Ma, while the mantle domain rocks finished that after 217.0 Ma. Supposed ductile faults with large displacements are robustly supported from the parallel ductile shear zones that separated the three metamorphic domains.

6.4. Implications for the Tectonic Origin of the CQMB

The aforementioned two models proposed two presumably reasonable interpretations of the genesis of the CQMB and its bearing HP-LT rocks in Central Qiangtang of North Tibet, i.e., the "Triassic suturing model" first put forward by *Li* [1987] and the "underthrusting and detachment model" by *Yin and Harrison* [2000]. The former envisages that the CQMB is the autochthonous accretionary complex generated from the Triassic northward subduction of the Paleo-Tethys beneath the North Qiangtang terrane and the subsequent thrusting over the South Qiangtang terrane [*Li*, 1987; *Li et al*., 1995, 2006; *Zhang et al*., 2006a, 2006b; *Zhai et al*., 2011a, 2011b; *Liang et al*., 2012]. The latter suggests that the lower crust of the middle and north Qiangtang is composed of the Triassic mélange of Jinsha suture zone to the north, which was emplaced after two coherent tectonic episodes including the earlier Triassic southward flat-slab subduction and the later Late Triassic–Early Jurassic extensional exhumation [*Yin and Harrison*, 2000; *Kapp et al*., 2003; *Pullen and Kapp*, 2014]. This heated controversy is, in part, the consequence of an inadequate grasp of established geologic relationships within and adjacent to the CQMB [*Pullen and Kapp*, 2014], especially for the HP-LT metamorphic rocks. Our new findings at Lanling (Figure 1) tend to support the "Triassic in situ suturing" hypothesis in terms of both the clear metamorphic zonation of the HP-LT rocks and the compiled comprehensive radiometric dating results.

First of all, the occurrence of gradually decreasing trend for individual peak metamorphic condition of core, mantle, and margin domains very probably negates the underthrusting and detachment model in that it is hard to imagine that the underthrusting basite or siliciclastic rocks were only subject to such low-temperature metamorphism as lower greenschist or Ep-amphibolite facies after drifting at lower crust over ~200 km by flat-slab subduction. If this hypothetically happened, the HP-LT rocks across the whole Lanling belt would display a relatively homogenous and high enough peak metamorphism, e.g., eclogitic facies. Combined with the observation that surrounding mélanges either in the west or east flank of Lanling show very similar geological features such as the nearly unmetamorphosed condition, N-S trending structural traces and the rock assemblage (Figure 2), a symmetric structural architecture on a scale of 10–20 km would be evidently demonstrated for the Lanling belt. This new discovery, however, is generally reconciled with the underthrusting and detachment model in the aspect that the contacting boundaries between the HP-LT rocks and their surrounding rocks everywhere within the CQMB are extensional low-angle normal faults [cf. *Yin and Harrison*, 2000; *Kapp et al*., 2003; *Pullen and Kapp*, 2014]. Nonetheless, note that it is a radical misconception to regard the Carboniferous–Triassic mélanges flanking the HP-LT rocks as sedimentary cover of the middle or entire Qiangtang terrane, which is denied by the recently performed detailed geological mappings, which alternatively clarified the whole CQMB as the accretionary complex of the Paleo-Tethys Ocean separating the North and South Qiangtang [cf. *Liang et al*., 2012, 2015]. We therefore infer that the block- or lense-like HP-LT rocks embedded within the CQMB were very likely exhumed by Late Triassic large-scale extensional detachment faulting in the background of a Triassic accretion-type orogen.

Second, our cautious compilation of the published radiometric results and revaluation on the Phg Ar-Ar dating results indicate that the HP-LT metamorphic rocks within the CQMB were exhumed to the upper crust after 222–217 Ma, which implies that the low-angle normal faulting supposedly started before Norian Age of Late Triassic. This argument forcefully precludes the prediction for the onset of crustal extension as Late Triassic–Early Jurassic [*Yin and Harrison*, 2000; *Kapp et al*., 2003; *Pullen and Kapp*, 2014]. Moreover, the metamorphic trajectory for the Grt-bearing blueschist of Lanling and eclogite within the CQMB [cf. *Zhai et al*., 2011b; *Liu et al*., 2011] never shows a clear two-staged metamorphism inherent to the

underthrusting and detachment model but coincides with a common retrograde process for the HP-LT rocks in oceanic subdcution zones [cf. *Tsujimori et al*., 2006; *Agard et al*., 2009].

7. Conclusion

The results of this study are as follows.

1. The Lanling high-pressure metamorphic belt in Central Qiangtang of North Tibet includes three shear zone that separated N-S trending metamorphic domains such as Grt-bearing blueschist core, epidote-blueschist mantle, and lower greenschist margin. Core and mantle domain blueschists are all characterized by hydrated metamorphic scenarios after peak metamorphism with heating plus depressurization trajectories.
2. Based on the compilation and reappraisal of the reported radiometric age data sets, a stepwise exhumation mode was put forward. The core domain eclogitic rocks were first exhumed onto shallower blueschist level during the period of 244–230 to 227.0–223.4 Ma. Subsequently, they were exhumed together starting at 223–220 Ma and finally entered the lower greenschist complex generally after 222–217 Ma.
3. HP-LT rocks in Central Qiangtang were probably exhumed in an extensional setting in the late stage of the northward subduction of the Paleo-Tethys Ocean which once separated the North and South Qiangtang terranes in Permian–Triassic. The Central Qiangtang metamorphic belt (CQMB) very likely represents an autochthonous accretionary complex of the Paleo-Tethys Ocean.

Acknowledgments

This work was jointly funded by the Young Scientist Fund of the National Natural Science Foundation of China (grant 41402177) and the Fundamental Research Funds for the Central Universities (2652014004). Our field work was supported by a project issued by the China Geological Survey (CGS): The integrated geological survey on the west part and central uplift of Qiangtang Block (grant 12120115026901). Data sets including the methods and results of the run experiments, the application of geothermobarometer, and the reinterpretation of previous Phg datings are available in the supporting information; any additional data may be obtained from X. Liang (e-mail: liangx@cugb.edu.cn). We are grateful to Gordon Lister and Marnie Forster for the assistance in argon diffusion modeling; the authors acknowledge the facilities, and the scientific and technical assistance, of the Australian Microscopy & Microanalysis Research Facility at the Centre of Advanced Microscopy, the Australian National University. Thanks to the two reviewers including Mauricio Ibanez-Mejia for their constructive comments and helpful suggestions on the manuscript.

References

Agard, P., P. Yamato, L. Jolivet, and E. Burov (2009), Exhumation of oceanic blueschists and eclogites in subductionzones: Timing and mechanisms, *Earth Sci. Rev.*, *92*, 53–79.

Bao, P. S., X. C. Xiao, J. Wang, C. Li, and K. Hu (1999), The blueschist belt in the Shuanghu Region, Central-Northern Tibet and its tectonic implications [in Chinese with English abstract], *Acta Geol. Sin.*, *73*(4), 302–314.

Bloch, E., J. Ganguly, R. Hervig, and W. J. Cheng (2015), ^{176}Lu–^{176}Hf geochronology of garnet I: Experimental determination of the diffusion kinetics of Lu^{3+} and Hf^{4+} in garnet, closure temperatures and geochronological implications, *Contrib. Mineral. Petrol.*, *169*, 12.

Cherniak, D. J., and E. B. Watson (2001), Pb diffusion in zircon, *Chem. Geol.*, *172*(1–2), 5–24.

Clarke, G. L., R. Powell, and J. A. Fitzherbert (2006), The lawsonite paradox: A comparison of field evidence and mineral equilibria modelling, *J. Metam. Geol.*, *24*(8), 715–725.

Deng, W. M., J. X. Yin, and Z. P. Yu (1996), The study of basic, ultra basic and volcanic rocks in Chabu–Shuanghu areas of Qiangtang, *Sci. China Ser. D*, *26*, 299–301.

Deng, X. G., L. Ding, X. H. Liu, A. Yin, P. A. Kapp, M. A. Murphy, and C. E. Manning (2000), Discovery of blueschists in Gangmari-Taoxing Co area, central Qiangtang, northern Tibet [in Chinese with English abstract], *Sci. Geol. Sin.*, *35*(2), 227–232.

Dong, Y. S., and C. Li (2009), Discovery of eclogite in the Guoganjianian Mountain, central Qiangtang area, northern Tibet, China [in Chinese with English abstract], *Geol. Bull. China*, *28*(9), 1197–1200.

Dong, Y. S., C. Li, J. R. Shi, and S. Y. Wang (2009), Retrograde metamorphism and tectonic emplacement of high pressure metamorphic belt in central Qiangtang Tibet [in Chinese with English abstract], *Acta Petrol. Sin.*, *25*(9), 2303–2309.

Dragovic, B., E. F. Baxter, and M. J. Caddick (2015), Pulsed dehydration and garnet growth during subduction revealed by zoned garnet geochronology and thermodynamic modeling, Sifnos, Greece, *Earth Planet. Sci. Lett.*, *413*, 111–122.

Foster, M. A., and G. S. Lister (2004), The interpretation of ^{40}Ar/^{39}Ar apparent age spectra produced by mixing: Application of the method of asymptotes and limits, *J. Struct. Geol.*, *26*, 287–305.

Foster, M. A., and G. S. Lister (2008), Tectonic sequence diagrams and the structural evolution of schists and gneisses in multiply deformed terranes, *J. Geol. Soc. Lond.*, *165*, 923–939.

Foster, M. A., and G. S. Lister (2014), ^{40}Ar/^{39}Ar geochronology and the diffusion of ^{39}Ar in phengite–muscovite intergrowths during step-heating experiments in vacuo, *J. Geol. Soc. Lond.*, *378*(1), 117–135.

Harrison, T. M., and O. S. Lovera (2014), The multi-diffusion domain model: Past, present and future, *Geol. Soc. Lond.*, *378*(1), 91–106.

Harrison, T. M., J. Célérier, A. B. Aikman, J. Hermann, and M. T. Heizler (2009), Diffusion of ^{40}Ar in muscovite, *Geochim. Cosmochim. Acta*, *73*, 1039–1051.

Hening, A. (1915), Zur Petrographie und geologie von Sudwest Tibet, in *Southern Tibet*, vol. 5, edited by S. Hedin, 220 pp., Norstedt, Stockholm.

Herwartz, D., C. Münker, E. E. Scherer, T. J. Nagel, J. Pleuger, and N. Froitzheim (2008), Lu-Hf garnet geochronology of eclogites from the balma Unit (Pennine Alps): Implications for Alpine paleotectonic reconstructions, *Swiss J. Geosci.*, *101*(suppl. 1), s173–s189.

Kapp, P., A. Yin, C. E. Manning, and T. M. Harrison (2003), Tectonic evolution of the early Mesozoic blueschist-bearing Qiangtang metamorphic belt, central Tibet, *Tectonics*, *22*(4), 1043, doi:10.1029/2002TC001383.

Li, C. (1987), The Longmucuo-Shuanghu-Lancangjiang plate suture and the north boundary of distribution of Gondwanafacies Permian-Carboniferous system in northern Xizang, China [in Chinese with English abstract], *J Changchun Uni. Earth Sci.*, *17*(2), 155–166.

Li, C., L. R. Chen, K. Hu, Z. R. Yang, and Y. R. Hong (1995), *Study on the Paleo-Tethys Suture Zone of Lungmu Co–Shuanghu, Tibet*, pp. 129–132, Geol. House, Beijing, China.

Li, C., Q. G. Zhai, W. Chen, J. J. Yu, X. P. Huang, and Y. Zhang (2006), Ar-Ar chronometry of the eclogite from central Qiangtang area,Qinghai-Tibet Plateau, *Acta Petrol. Sin.*, *22*(12), 2843–2849.

Li, C., Y. S. Dong, Q. G. Zhai, J. J. Yu, and X. P. Huang (2008), High- pressure metamorphic belt in Qiangtang, Qinghai- Tibet Plateau, and its tectonic significance, *Geol. Bull. China*, *27*(1), 27–35.

Li, C., G. Y. Zhai, L. Q. Wang, and X. C. Mao (2009), An important window for understanding the Qinghai-Tibet Plateau: A review on research progress in recent years of Qiangtang area, Tibet, China [in Chinese with Englishabstract], *Geol. Bull. China*, *28*(9), 1169–1177.

Li, G. M., J. X. Li, J. X. Zhao, K. Z. Qin, M. J. Cao, and N. J. Evans (2015), Petrogenesis and tectonic setting of Triassic granitoids in the Qiangtang terrane, central Tibet: Evidence from U–Pb ages, petrochemistry and Sr–Nd–Hf isotopes, *J. Asian Earth Sci.*, *105*, 443–453.
Li, Y. J., H. R. Wu, and H. S. Li (1997), Discovery of radioarians in the Amugang and Chasang Groups and Lugu Formation in northern Tibet and some related geological problems, *Geogr. Rev.*, *43*(3), 250–256.
Liang, X., G. H. Wang, G. L. Yuan, and Y. Liu (2012), Structural sequence and geochronology of the Qomo Ri accretionary complex, Central Qiangtang, Tibet: Implications for the Late Triassic subduction of the Paleo-Tethys Ocean, *Gondw. Res.*, *22*(2), 470–481.
Liang, X., G. H. Wang, G. L. Yuan, and X. C. Che (2015), Mesozoic and Cenozoic deformations in the Raggyorcaka area, Tibet: Implications for the tectonic evolution of the North Qiangtang terrane, *J. Geol. Soc.*, *172*, 614–623.
Lister, G. S., and M. A. Forster (2016), White mica $^{40}Ar/^{39}Ar$ age spectra and the timing of multiple episodes of high-P metamorphic mineral growth in the Cycladic eclogite–blueschist belt, Syros, Aegean Sea, Greece, *J. Metam. Geol.*, *1–21*.
Liu, Y., M. Santosh, Z. B. Zhao, W. C. Niu, and G. H. Wang (2011), Evidence for Palaeo-Tethyan oceanic subduction within central Qiangtang, *Lithos*, *127*, 39–53.
Lu, B., C. Y. Liu, Z. Liu, and Y. T. Li (2001), Basement formation and structural features of the Qiangtang basin and their implications, *Seismol. Geol.*, *23*(4), 510–517.
Lu, J. P., N. Zhang, W. H. Huang, Z. H. Tang, Y. K. Li, H. Xu, Q. E. Zhou, G. Lu, and Q. Li (2006), Characteristics and significance of the metamorphic minerals glaucophane-lawsonite assemblage in the Hongjishan area, north-central Qiangtang, northern Tibet, China [in Chinese with English abstract], *Geol. Bull. China*, *25*(1), 70–75.
Massonne, H. J., and W. Schreyer (1987), Phengite geobarometry based on the limiting assemblage with K-feldspar, phlogopite, and quartz, *Contrib. Mineral. Petrol.*, *96*, 212–224.
McDougal, I., and T. M. Harrison (1999), *Geochronology and Thermochronology by the $^{40}Ar/^{39}Ar$ Method*, pp. 1–269, Oxford Univ. Press.
Pullen, A., and P. Kapp (2014), Mesozoic tectonic history and lithospheric structure of the Qiangtang terrane: Insights from the Qiangtang metamorphic belt, central Tibet, *Geol. Soc. Am. Spec. Pap.*, *507*.
Pullen, A., P. Kapp, G. E. Gehrels, J. D. Vervoort, and L. Ding (2008), Triassic continental subduction in central Tibet and Mediterranean-style closure of the Paleo-Tethys Ocean, *Geology*, *36*(5), 351–354.
Scherer, E. E., K. L. Cameron, and J. Blichert-Toft (2000), Lu–Hf garnet geochronology: Closure temperature relative to the Sm–Nd system and the effects of trace mineral inclusions, *Geochim. Cosmochim. Acta*, *64*(19), 3413–3432.
St-Onge, M. R., N. Rayner, R. M. Palin, M. P. Searle, and D. J. Waters (2013), Integrated pressure–temperature–time constraints for the Tso Morari dome (Northwest India): Implications for the burial and exhumation path of UHP units in the western Himalaya, *J. Metam. Geol.*, *31*(5), 469–504.
Tang, X. C., and K. J. Zhang (2014), Lawsonite- and glaucophane-bearing blueschists from NW Qiangtang, northern Tibet, China: Mineralogy, geochemistry, geochronology, and tectonic implications, *Int. Geol. Rev.*, *56*(2), 150–166.
Tomkins, H. S., R. Powell, and D. J. Ellis (2007), The pressure dependence of the zirconium-in-rutile thermometer, *J. Metam. Geol.*, *25*, 703–713.
Tsujimori, T., V. B. Sisson, J. G. Liou, G. E. Harlow, and S. S. Sorensen (2006), Very-low-temperature record of the subduction process: A review of worldwide lawsonite eclogites, *Lithos*, *92*, 609–624.
Wang, C. S., H. S. Yin, and Y. Li (2001), *The Geological Evolution and Prospective Oil and Gas Assessment of the Qiangtang Basin in Northern Tibetan Plateau*, pp. 1–170, Geol. House, Beijing, China.
Wang, G. H., F. L. Han, Y. J. Yang, Y. Q. Li, and J. L. Cui (2009), Discovery and geologic significance of Late Paleozoic accretionary complexes in central Qiangtang, northern Tibet, China [in Chinese with English abstract], *Geol. Bull. China*, *28*(9), 1181–1187.
Wang, J., F. W. Tan, and Y. L. Li (2004), *The Potential of the Oil and Gas Resources in Major Sedimentary Basins on the Qinghai-Tibet Plateau*, pp. 1–100, Geological Publishing House, Beijing, China.
Yin, A., and T. M. Harrison (2000), Geological evolution of the Himalayan-Tibetan Orogen, *Annu. Rev. Earth Planet. Sci. Lett.*, *28*, 211–263.
Zhai, Q. G., C. Li, J. Wang, W. Chen, and Y. Zhang (2009a), Petrology, mineralogy and ^{40}Ar-^{39}Ar chronology for Rongma blueschist from Central Qiangtang, northern Tibet [in Chinese with English abstract], *Acta Petrol. Sin.*, *25*(9), 2281–2288.
Zhai, Q. G., J. Wang, and Y. Wang (2009b), Discovery of eclogite at Gangmacuo area from Gerze County, Tibet, China, *Geol. Bull. China*, *28*(12), 1720–1724.
Zhai, Q. G., R. Y. Zhang, B. M. Jahn, C. Li, S. G. Song, and J. Wang (2011a), Triassic eclogites from central Qiangtang, northern Tibet, China: Petrology, geochronology and metamorphic P-T path, *Lithos*, *125*(1), 173–189.
Zhai, Q. G., B. M. Jahn, R. Y. Zhang, J. Wang, and L. Su (2011b), Triassic Subduction of the Paleo-Tethys in northern Tibet, China: Evidence from the geochemical and isotopic characteristics of eclogites and blueschists of the Qiangtang Block, *J. Asian Earth Sci.*, *42*, 1356–1370.
Zhai, Q. G., B. M. Jahn, L. Su, R. E. Ernst, K. L. Wang, R. Y. Zhang, J. Wang, and S. H. Tang (2013), SHRIMP zircon U-Pb geochronology, geochemistry and Sr-Nd-Hf isotopic compositions of a mafic dyke swarm in the Qiangtang terrane, northern Tibet and geodynamic implications, *Lithos*, *174*, 28–43.
Zhang, K. J., J. X. Cai, and Y. X. Zhang (2006a), Eclogites from central Qiangtang, northern Tibet (China) and tectonic implications, *Earth Planet. Sci. Lett.*, *245*, 722–729.
Zhang, K. J., Y. X. Zhang, B. Li, Y. T. Zhu, and R. Z. Wei (2006b), The blueschist-bearing Qiangtang metamorphic belt (northern Tibet, China) as an in situ suture zone: Evidence from geochemical comparison with the Jinsa suture, *Geology*, *34*, 493–496.
Zhang, X. Z., Y. S. Dong, J. R. Shi, and S. Y. Wang (2010a), The formation and significance of jadeite garnet mica schist newly discovered in Longmu Co-Shuanghu suture zone, Central Qiangtang [in Chinese with English abstract], *Earth Sci. Front.*, *17*(1), 93–103.
Zhang, X. Z., Y. S. Dong, C. Li, W. Chen, J. R. Shi, Y. Zhang, and S. Y. Wang (2010b), Identification of the eclogites with different ages and their tectonic significance in central Qiangtang, Tibetan Plateau: Constraints from ^{40}Ar-^{39}Ar geochronology [in Chinese with English abstract], *Geol. Bull. China*, *29*(12), 1815–1824.
Zhao, Z. Z., and Y. T. Li (2000), Conditions of petroleum geology of the Qiangtang basin of the Qinghai-Tibet plateau, *Acta Geol. Sin.*, *74*(3), 661–665.
Zhao, Z. Z., P. D. Bons, G. H. Wang, Y. Liu, and Y. L. Zheng (2014), Origin and pre-Cenozoic evolution of the south Qiangtang basement, Central Tibet, *Tectonophysics*, *623*(7), 52–66.
Zhu, T. X., Q. Y. Zhang, X. T. Feng, H. Dong, Y. S. Yu, and H. R. Li (2010), $^{40}Ar/^{39}Ar$ isotopic dating of the glaucophane in CaiduoCaka, Central Qiangtang area, Northern Tibet, China and its geological significance, *Acta Geol. Sin.*, *84*(10), 1448–1456.